Chen-2015-Viscoelasticity of Reversible Gelation for Ionomers

DATASET · OCTOBER 2015

4 AUTHORS, INCLUDING:

R. A. Weiss
University of Akron
227 PUBLICATIONS **5,209** CITATIONS

SEE PROFILE

Macromolecules

Article

pubs.acs.org/Macromolecules

Viscoelasticity of Reversible Gelation for Ionomers

Quan Chen,*[,†] Chongwen Huang,[‡] R. A. Weiss,[‡] and Ralph H. Colby[†]

[†]Department of Materials Science and Engineering The Pennsylvania State University, University Park, Pennsylvania 16802, United States

[‡]Department of Polymer Engineering University of Akron, Akron, Ohio 44325, United States

Supporting Information

ABSTRACT: Linear viscoelasticity (LVE) of low-ion-content and low-molecular-weight (nonentangled) randomly sulfonated polystyrene shows a sol−gel transition when the average number of ionic groups per chain approaches unity. This transition can be well understood by regarding the number of ionizable sites over a chain as the relevant functionality for cross-linking. For ionomers below but very close to the gel point, the LVE shows power law relaxation similar to gelation of chemical cross-linking. Nevertheless, ionomers near and beyond the gel point also show terminal relaxation not seen in chemically cross-linking systems, which is controlled by ionic dissociation. Careful analysis of the power law region of the frequency dependence of complex modulus close to the gel point shows a change in exponent from ∼1 at high frequency to ∼0.67 at low frequency, which strongly suggests a transition from mean-field to critical percolation known as the Ginzburg point. A mean-field percolation theory by Rubinstein and Semenov for gelation with effective breakup has been modified to include critical percolation close to the gel point and predicts well the observed LVE of lightly sulfonated polystyrene oligomers.

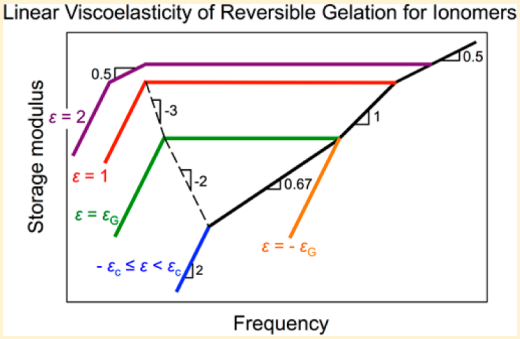

1. INTRODUCTION

It is well-known that "gel" is a phenomenological term with diverse applications.[1,2] Flory classified gels into four groups based on their structure: (1) self-assembled gels with ordered structures, (2) covalently cross-linked disordered polymer gels, (3) disordered polymer gels formed by physical aggregation/association, and (4) particulate disordered gels. The distinction between the chemical gels (class 2) and physical gels (class 3) is that the physical gel is thermally reversible and ultimately flows as a liquid while the chemical gel has permanent cross-links. As a result, physical gels are similar to chemical gels in a certain time and temperature range where the physical aggregation/association is stable.[2,3] Ionomers that form reversible gels are useful as hot melt adhesives.[4,5]

The gel point usually characterizes the liquid-to-solid transformation and network formation during the chemical cross-linking. As the gel point is approached, the large clusters percolate over the system, leading to divergence of the viscosity.[3] The gel point is well-defined for chemical cross-linking of long precursor chains, usually referred to as vulcanization.[3] Assume each precursor chain has f cross-linkable sites, the mean-field prediction of the gel point is $p_c = 1/(f - 1)$. In previous work,[6] an analogous gel point was noted for ionomer chains: *Regarding each monomer of a styrene chain as a cross-linkable site via random sulfonation,* the fraction of ionized (sulfonated) monomer p for a precursor chain having N monomers at the gel point is

$$p_c = 1/(N - 1) \tag{1}$$

corresponding to an average of one sulfonate per precursor chain.[3] The relative extent of reaction is defined as

$$\varepsilon = (p - p_c)/p_c \tag{2}$$

with $\varepsilon < 0$ below the gel point, $\varepsilon = 0$ at the gel point, and $\varepsilon > 0$ beyond. The gel fraction P_{gel} is the order parameter of this connectivity transition, 0 below the gel point, while above the gel point $P_{gel} \sim \varepsilon$, which approaches 0 at the gel point, meaning the system is still occupied only by sol at the gel point, while fully occupied by gel at $\varepsilon = 1$ ($p = 2p_c$).

The gel point estimated by eq 1 is supported by the linear viscoelastic complex modulus reported by Weiss and co-workers.[7,8] For random sulfonated oligomeric styrene with low molecular weight M = 4000 g/mol (N = 38) (< entanglement molecular weight M_e = 17 000 g/mol), the gel point is expected to be $p_c = 1/(N - 1)$ = 2.7 mol %. In accordance with this expectation, the ionomer having p = 2.5 mol % ($\varepsilon = -0.064$) shows power law viscoelasticity usually seen quite close to the gel point. In comparison, the samples with p = 4.8 mol % (ε = 0.80) and 6.5 mol % (ε = 1.4) exhibit a well-defined plateau before terminal relaxation, suggesting the samples are beyond the gel point and are reversible gels.

To better understand the sol−gel transition, the linear viscoelasticity of these samples is examined based on the mean-

Received: November 11, 2014
Revised: December 31, 2014
Published: February 6, 2015

DOI: 10.1021/ma502280g
Macromolecules 2015, 48, 1221−1230

field theory of Rubinstein and Semenov.[6,9,10] The theory predicts qualitatively the relaxation behavior. However, one apparent deviation is noted; the frequency dependence of storage modulus for the 2.5 mol % sample exhibits power-law viscoelasticity, but the power differs from that predicted by the mean-field theory. This difference encourages us to question the validity of the mean-field assumption.

In general, the mean-field theory is applicable when there is considerable overlapping of chains.[3] At $p = 0$ and $\varepsilon = -1$, a precursor chain of N segments and size $R \sim N^{1/2}$ has a self-concentration $\sim N/R^3 \sim N^{-1/2} < 1$ within its pervaded volume, meaning $N^{1/2}$ chains overlap in a pervaded volume in the melt. This number decreases as the gel point is approached and reaches unity at $-\varepsilon_G = -N^{-1/3}$ known as the Ginzburg point, meaning clusters/strands are at their overlap concentration when ε is close enough to the gel point, i.e., $-\varepsilon_G < \varepsilon < \varepsilon_G$, where critical percolation applies.[3] A transition from mean-field to critical percolation can be seen if N is neither too large, where mean-field percolation should dominate, nor too small, where critical percolation should dominate. In this study, this transition is critically tested by changing the length of precursor PS chain N and the extent of sulfonation p. There is strong evidence of this transition utilizing the precursor polystyrene (PS) chain having M = 13 500 g/mol (N = 130) with ionic content very close to $p_c = 1/(N-1) = 0.78$ mol %. Since M here is smaller than M_e (= 17 000 g/mol), the number of other chains within each chain's pervaded volume is smaller than the threshold for entanglement. This number decreases with p approaching p_c,[3] meaning that the effect of entanglements is negligible, even when the average M per cluster/strand becomes very large for p close to p_c.

The mean-field theory of Rubinstein and Semenov is modified by including a critical percolation region for $-\varepsilon_G < \varepsilon < \varepsilon_G$ in section 2. The modified theory can well predict the linear viscoelasticity of almost all the short lightly sulfonated styrene oligomers studied so far. Section 3 provides experimental details, and section 4 compares theory with experiment.

2. THEORY

In this section percolation theory for gelation is quickly reviewed, including mean-field theory and critical percolation closer to the gel point, as though all bonds are permanent. Then Rubinstein and Semenov's idea for effective breakup in mean field is reviewed and extended to include critical percolation closer to the gel point.

2.1. Dynamics below the Gel Point. For samples below both the gel point and the Ginzburg point ($\varepsilon < -\varepsilon_G$), the molecular weight of the largest cluster M_{char} increases with ε. The precursor chain has molecular weight $M_X = M_0 N_X$, size $R_X = N_X^{1/2} b$, and Rouse relaxation time $\tau_X = \tau_0 N_X^2$, with b the segmental size, N_X the number of segments, M_0 the segment molecular weight, and τ_0 the relaxation time of one segment. The mean-field theory gives the largest cluster having molecular weight M_{char} and size ξ_{char}:

$$M_{char} = M_X|\varepsilon|^{-2} \tag{3}$$

$$\xi_{char} = R_X(M_{char}/M_X)^{1/D} = R_X|\varepsilon|^{-1/2} \tag{4}$$

where D (= 4 in the mean-field gelation theory[3]) is the fractal dimension so that the size of a cluster having molecular weight M is $R/R_X = (M/M_X)^{1/D}$. Since the precursor chain is short, the Rouse relaxation time,[9−11] $\tau_{char} \sim M_{char}\xi_{char}^2 \sim M_{char}^{1+2/D}$, is used so that

$$\tau_{char} = \tau_X(M_{char}/M_X)^{1+2/D} = \tau_X|\varepsilon|^{-3} \tag{5}$$

The terminal relaxation modulus in this region is

$$G \cong \nu kT|\varepsilon|^3 \tag{6}$$

where ν is the number density of precursor chains. The mean-field theory holds until the Ginzburg point $\varepsilon_G = N_X^{-1/3}$, where the characteristic clusters no longer overlap and the mean-field scaling no longer holds, meaning that eqs 3−6 hold only for $\varepsilon < -\varepsilon_G$.

The molecular weight, chain size, characteristic time, and terminal modulus of the cluster at the Ginzburg point can be obtained by inputting $\varepsilon_G = N_X^{-1/3}$ into eqs 3−6 to obtain[11]

$$M_G = M_X\varepsilon_G^{-2} = M_X N_X^{2/3} \tag{7}$$

$$\xi_G = R_X(M_G/M_X)^{1/D} = R_X N_X^{1/6} \tag{8}$$

$$\tau_G = \tau_X(M_G/M_X)^{1+2/D} = \tau_X N_X \tag{9}$$

$$G_G = \nu kT N_X^{-1} \tag{10}$$

Further increasing ε from $-\varepsilon_G$ ($-\varepsilon_G \le \varepsilon < 0$) leads to critical percolation of Ginzburg blobs[3,12,13]

$$M_{char} \cong M_G|\varepsilon/\varepsilon_G|^{-1/\sigma} = M_G|\varepsilon/\varepsilon_G|^{-2.2} \tag{11}$$

$$\xi_{char} \cong \xi_G|\varepsilon/\varepsilon_G|^{-\nu} = \xi_G|\varepsilon/\varepsilon_G|^{-0.88} \tag{12}$$

$$\tau_{char} \cong \tau_G|\varepsilon/\varepsilon_G|^{-2\nu-1/\sigma} = \tau_G|\varepsilon/\varepsilon_G|^{-4.0} \tag{13}$$

$$G \cong G_G|\varepsilon/\varepsilon_G|^{(2\nu+1/\sigma)\times 0.67} = G_G|\varepsilon/\varepsilon_G|^{2.7} \tag{14}$$

For $-\varepsilon_G < \varepsilon < 0$, the relaxation time of the characteristic cluster increases with ε and diverges at the gel point (as ε approaches 0). In section 2.3 the relaxation time with reversible associations will be shown to have a maximum possible value set by effective breakup.

2.2. Dynamics above the Gel Point. In the following discussion, the $1 \le \varepsilon$ case is first considered, where all chains are involved in the gel, second $\varepsilon_G \le \varepsilon < 1$ where the system is mixture of sol and gel and mean-field percolation holds, and third $0 \le \varepsilon < \varepsilon_G$ where the system is mixture of sol and gel and critical percolation holds.

At $p \ge 2p_c$ ($1 \le \varepsilon$), all the chains are involved in the network whose modulus is proportional to the number density of network strands. Considering that p_c corresponds to an average of one sticker per precursor chain, the number of ionic groups per precursor chain is p/p_c, and the average number of network strands per precursor chain is $N_s = p/p_c - 1 \equiv \varepsilon$. Replacing N_s with ε in the sticky Rouse model[14−16] predicting $G_N \approx \nu kTN_s$ and $\tau_{chain} \approx \tau_s N_s^2$

$$G_N = \nu kT\varepsilon \quad \text{for } p \ge 2p_c \tag{15}$$

$$\tau_{chain} \approx \tau_s\varepsilon^2 \quad \text{for } p \ge 2p_c \tag{16}$$

At $p = 2p_c$ and $\varepsilon = 1$, the plateau modulus recovers to the familiar result $G_N \approx \nu kT$ and relaxation time is simply the sticker lifetime τ_s.

Above the Ginzburg point while below $\varepsilon \sim P_{gel} = 1$ ($\varepsilon_G \le \varepsilon < 1$), the molecular weight of the network strand M_{strand} decreases with increasing ε. The mean-field theory holds, and the

DOI: 10.1021/ma502280g
Macromolecules 2015, 48, 1221−1230

network strands have molecular weight, size, and characteristic Rouse time:[13]

$$M_{strand} = M_X \varepsilon^{-2} \tag{17}$$

$$\xi_{strand} = R_X (M_{strand}/M_X)^{1/D} = R_X \varepsilon^{-1/2} \tag{18}$$

$$\tau_{strand} = \tau_X (M_{strand}/M_X)^{1+2/D} = \tau_X \varepsilon^{-3} \tag{19}$$

The plateau modulus in this mean-field percolation region is

$$G \cong G_G (\varepsilon/\varepsilon_G)^3 = \nu kT \varepsilon^3 \tag{20}$$

The modulus recovers to G_G at ε_G and νkT at $\varepsilon = 1$.

Below the Ginzburg point ($0 \leq \varepsilon < \varepsilon_G$), critical percolation holds, leading to formation of gel with strands of molecular weight, size, and Rouse time

$$M_{strand} \cong M_G (\varepsilon/\varepsilon_G)^{-1/\sigma} = M_G (\varepsilon/\varepsilon_G)^{-2.2} \tag{21}$$

$$\xi_{strand} \cong \xi_G (\varepsilon/\varepsilon_G)^{-\nu} = \xi_G (\varepsilon/\varepsilon_G)^{-0.88} \tag{22}$$

$$\tau_{strand} \cong \tau_G (\varepsilon/\varepsilon_G)^{-2\nu-1/\sigma} = \tau_G (\varepsilon/\varepsilon_G)^{-4.0} \tag{23}$$

The plateau modulus of the gel in this region is

$$G \cong G_G (\varepsilon/\varepsilon_G)^{(2\nu+1/\sigma)\times 0.67} = G_G (\varepsilon/\varepsilon_G)^{2.7} \tag{24}$$

Equations 21−24 are perfectly symmetric with eqs 11−14 for $-\varepsilon_G \leqslant \varepsilon < 0$. The relaxation time of the reversible gel always relies on the *effective breakup of strands*. The symmetry between the structure of a gel strand at $\varepsilon > 0$ and that of a cluster at $\varepsilon < 0$ allows an estimation of effective breakup time in both mean-field percolation and critical percolation regions, as explained next.

2.3. Effective Breakup. The discussion in section 2.1 (below the gel point) and section 2.2 (above the gel point) holds perfectly for permanent chemical bonds,[3,10,11] but reversible gels are always viscoelastic liquids and only act as permanent gels on time scales shorter than the sticker lifetime. On longer time scales both larger clusters and the reversible network relax by a pathway that Rubinstein and Semenov[9,10] term effective breakup, wherein large clusters (or gel strands) break into two smaller parts of comparable size. While the relaxation time of the characteristic cluster (eqs 5 and 13) and the network strand (eqs 19 and 23) get longer as the gel point is approached, the effective breakup time *decreases* as the gel point is approached because more breakable sites are present in larger clusters/strands.

For mean-field percolation Rubinstein and Semenov[9,10] clearly discuss effective breakup, since intramolecular associations (loops) are not formed when clusters strongly overlap each other. Effective breakup occurs for reversible cross-links on the backbone instead of the side branches of a cluster or strand (if they break no stress is relaxed) as schematically shown in Figure 1. For critical percolation, however, there are loops and multiple backbones per cluster or strand. For this case, the effective breakup sites are not so well-defined.

The (red) backbone of the mean-field percolation cluster or gel strand is a random walk of connected precursor chains with molecular weight

$$M_{bb} = M_X (\xi_{strand}/R_X)^2 = M_X \varepsilon^{-1} \tag{25}$$

so there are $M_{bb}/M_X = 1/\varepsilon$ reversible bonds in this backbone that could break. The relaxation of the strand relies on effective breakup corresponding to lifetime:

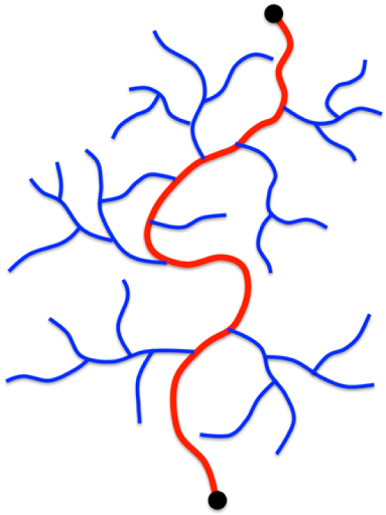

Figure 1. Scheme of a cluster/strand formed via mean-field percolation. Since there are no loops, effective breakup sites are reversible cross-links on the backbone (in red) instead of branches (in blue). In critical percolation, however, there are loops and multiple backbones on each gel strand, making the effective breakup sites harder to define. The cluster with equal effective breakup time and relaxation time is defined as the critical cluster[9,10] that controls the terminal relaxation near the gel point (both below and above).

$$\tau_{life} = \tau_s M_X / M_{bb} = \tau_s \varepsilon \tag{26}$$

At the gel point ($\varepsilon = 0$) the lifetime is very short because the very long backbone has many reversible bonds that could break. This lifetime increases beyond the gel point and recovers to τ_s at $\varepsilon = 1$, where all precursor chains connect to the gel. The concept of effective breakup, introduced by Rubinstein and Semenov, is where this lifetime (vanishing at the gel point, eq 26) equals the Rouse relaxation time of the characteristic cluster (diverging at the gel point, eq 5) or gel strand (eq 19), corresponding to a critical extent of reaction $\varepsilon_c = (\tau_X/\tau_s)^{1/4}$ and the effective breakup relaxation time is obtained by substituting this critical extent of reaction into eq 5, 19, or 26.

$$\tau_c = \tau_X^{1/4} \tau_s^{3/4} \tag{27}$$

Closer to the gel point than the critical extent of reaction ε_c, the gel strands and characteristic clusters are larger but they need to break to the same scale (with the same effective breakup time as eq 27) in order to relax. At τ_c, the characteristic modulus would be

$$G_c = \nu kT \tau_X^{3/4} \tau_s^{-3/4} \tag{28}$$

This is the essence of Rubinstein and Semenov's argument, which assumes $\varepsilon_c > \varepsilon_G$ so that this breakup acts on mean-field percolation clusters and strands. If, on the other hand, $\varepsilon_c < \varepsilon_G$, then the breakup acts on critical percolation clusters, whose statistics and dynamics have different scalings with extent of reaction, as partially discussed above.

Critical percolation forms loops in the red backbone of Figure 1, complicating the derivation of τ_c. Figure 8 will show that eq 27 also holds for $\varepsilon_c < \varepsilon_G$, which is rationalized in an argument in the Appendix. Then, the terminal modulus G_c at effective breakup can be evaluated as

$$G_c = G_G (\tau_G/\tau_c)^{0.67} = \nu kT N_X^{-1/3} (\tau_X/\tau_s)^{0.5} \tag{29}$$

DOI: 10.1021/ma502280g
Macromolecules 2015, 48, 1221−1230

For $\varepsilon_c \le \varepsilon < \varepsilon_G$, $\tau_c = \tau_X^{1/4}\tau_s^{3/4}$ leads to the effective breakup time of a gel strand scaling with plateau modulus $\tau_{life} \sim G^{1/2}$, as derived in the Appendix. Combining this scaling with eq 24 and $\tau_{life} = \tau_s\varepsilon_G$ at ε_G (eq 26) gives

$$\tau_{life} \cong \tau_s\varepsilon_G(\varepsilon/\varepsilon_G)^{1.35} = \tau_s N_X^{-1/3}(\varepsilon/\varepsilon_G)^{1.35} \quad (30)$$

Changes of (a) terminal relaxation time τ and (b) modulus G with ε are summarized in Figure 2, and the storage modulus

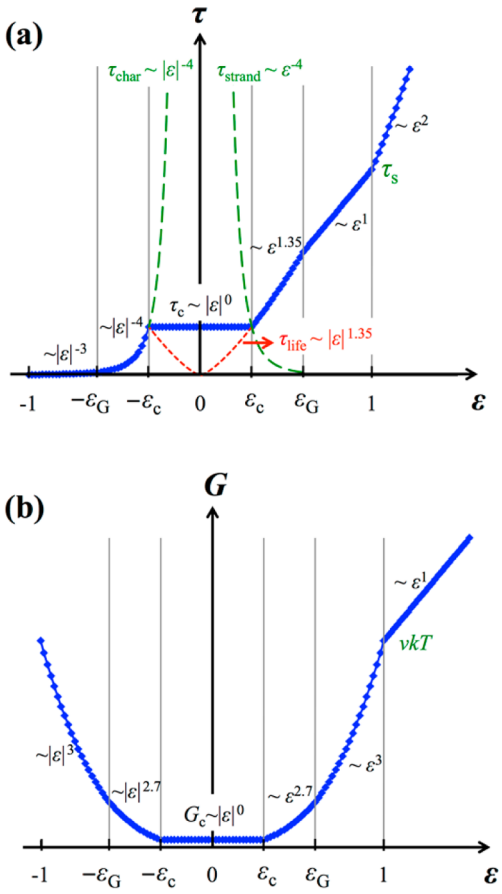

Figure 2. Schematic illustration of (a) terminal relaxation time and (b) terminal relaxation modulus as functions of relative extent of sulfonation ε in the case of $\varepsilon_c < \varepsilon_G$.

against angular frequency ω is summarized in Figure 3: (1) For $-1 < \varepsilon < -\varepsilon_G$, clusters are formed via mean-field percolation, and the relaxation time relies on the Rouse relaxation having $\tau_{char} \sim |\varepsilon|^{-3}$ (eq 5, see Figure 2a) and $G \sim |\varepsilon|^3$ (eq 6, see Figure 2b), leading to $G' \sim \omega$ (see Figure 3) before the terminal relaxation. (2) For $-\varepsilon_G \le \varepsilon < -\varepsilon_c$, critical percolation applies but the gel has not yet formed. The relaxation is still Rouse type to give $\tau_{char} \sim |\varepsilon|^{-4}$ (eq 13, see Figure 2a), $G \sim |\varepsilon|^{2.7}$ (eq 14, see Figure 2b), and $G' \sim \omega^{0.67}$ (= 2.7/4) (see Figure 3) before the terminal relaxation. The terminal relaxation time changes more significantly with ε than in region 1 because a more open structure is formed via critical percolation than via mean-field percolation. The exponent 0.67 is a signature of the Rouse model for critical percolation.[3,12] (3) The relaxation time and effective breakup time coincide at ε_c. Thus, in a region $-\varepsilon_c \le \varepsilon < \varepsilon_c$, the clusters/strands larger than those at ε_c have effective breakup time shorter than their intact Rouse relaxation time. Then, the effective breakup occurs continuously (before τ_c) until the subclusters/strands reach a critical cluster/strand size,

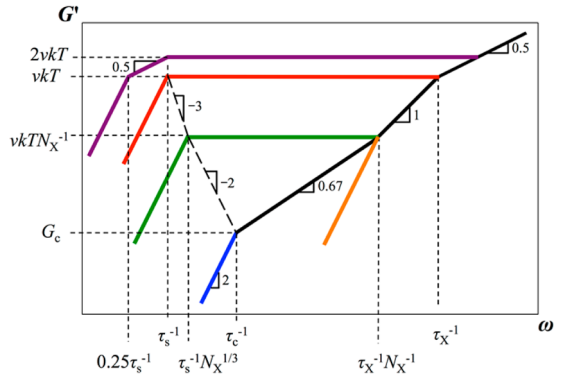

Figure 3. Schematic illustration of storage modulus $G'(\omega)$ during the gelation of reversible gels on logarithmic scales for $\varepsilon_c < \varepsilon_G$. Terminal modulus and terminal relaxation ($G' \sim \omega^2$) are highlighted in color for five cases: Orange is below the gel point at $\varepsilon = -\varepsilon_G$. Blue is close to the gel point with $-\varepsilon_c \le \varepsilon < \varepsilon_c$ where the effective breakup keeps relaxation time constant. Green is above the gel point at $\varepsilon = \varepsilon_G$. Red is at $\varepsilon = 1$ where all sol clusters have attached to the gel. Purple is at $\varepsilon = 2$, further above the gel point. The dashed lines connecting terminal tails $-\varepsilon_c \le \varepsilon < \varepsilon_c$ (blue), $\varepsilon = \varepsilon_G$ (green), and $\varepsilon = 1$ indicate scaling of terminal relation modulus with terminal relaxation time in regions of $\varepsilon_c \le \varepsilon < \varepsilon_G$ where $G \sim \tau_{life}^2$ and $\varepsilon_G \le \varepsilon < 1$ where $G \sim \tau_{life}^3$.

which then relax immediately (at τ_c). Therefore, for $-\varepsilon_c \le \varepsilon < \varepsilon_c$, the relaxation time and modulus remain the same, i.e., τ_c (eq 27, see Figure 2a) and G_c (eq 29, see Figure 2b). (4) For $\varepsilon_c \le \varepsilon < \varepsilon_G$, the gel starts to manifest as a plateau of G', and the relaxation of gel strands is governed by effective breakup of clusters formed by critical percolation to give $\tau \sim |\varepsilon|^{1.35}$ (eq 30, see Figure 2a) and $G \sim |\varepsilon|^{2.7}$ (eq 24, see Figure 2b). In this region, the terminal relaxation modulus changes with terminal relaxation time as $G \sim \tau^2$ (see Figure 3). (5) For $\varepsilon_G \le \varepsilon < 1$, the degree of gelation increases with ε and the system is still a mixture of gel and sol to give plateau modulus smaller than vkT ($G \approx vkT$ at $\varepsilon = 1$), and the relaxation of gel strands is governed by effective breakup of mean-field percolation clusters with $\tau \sim \varepsilon$ (eq 26, see Figure 2a) and $G \sim \varepsilon^3$ (eq 20, see Figure 2b). The terminal relaxation modulus changes with terminal relaxation time as $G \sim \tau^3$ (see Figure 3). (6) Finally, for $\varepsilon > 1$, all the chains are involved in the gel to have plateau modulus larger than vkT and increasing with ε. The strands between ionic groups become the gel strands, with $\tau \approx \tau_s\varepsilon^2$ (see Figure 2a) and $G \approx vkT\varepsilon$ (see Figure 2b), leading to sticky-Rouse type relaxation (see Figure 3).

2.3. Theoretical Expression of Complex Modulus in Terms of Frequency. The theory in sections 2.1 and 2.2 is based on scaling. The frequency dependence of complex modulus can be written as eqs 31−36.

$$G^*(\omega) = G_X^*(\omega) + G_{MF}^*(\omega) = i\omega vkT\left[\sum_{p=2}^{N_X}\frac{\tau_X/p^2}{1 + i\omega\tau_X/p^2} + \int_{\tau_X}^{\infty}\frac{(\tau_X/\tau)^1}{i\omega + 1/\tau_{char} + 1/\tau}\frac{d\tau}{\tau}\right] \quad (\varepsilon < -\varepsilon_G) \quad (31)$$

For $\varepsilon < -\varepsilon_G$, the cluster is formed by mean-field percolation, and thus the complex modulus has contributions from the Rouse relaxation of the precursor chains (subscript "X" embodied in the sum) and Rouse relaxation of mean-field percolation clusters (subscript "MF" embodied in the integral). The Rouse relaxation of the precursor chains ends at the second mode ($p = 2$) simply because the first mode has been

DOI: 10.1021/ma502280g
Macromolecules 2015, 48, 1221−1230

incorporated in the MF integral. For the MF part, the relaxations start at τ_X and end at τ_{char}, and $G^*(\omega) \sim (i\omega)^u$ with $u = 1$. Considering these conditions, the MF part of the modulus is written as integration of $(\tau_{startup}/\tau)^u/[i\omega + 1/\tau_{cutoff} + 1/\tau]$ in eq 31, where integrand $((\tau_{startup}/\tau)^u/[i\omega + 1/\tau_{cutoff} + 1/\tau])$ is commonly written for both mean-field and critical percolation parts in eqs 32−35.

$$G^*(\omega) = G_X^*(\omega) + G_{MF}^*(\omega) + G_{CP}^*(\omega)$$
$$= i\omega vkT\left[\sum_{p=2}^{N_X} \frac{\tau_X/p^2}{1 + i\omega\tau_X/p^2} + \frac{N_X - 1}{N_X}\int_{\tau_X}^{\infty} \frac{(\tau_X/\tau)^1}{i\omega + 1/\tau_G + 1/\tau}\frac{d\tau}{\tau} + \frac{0.67}{N_X}\int_{\tau_G}^{\infty} \frac{(\tau_G/\tau)^{0.67}}{i\omega + 1/\tau_{char} + 1/\tau}\frac{d\tau}{\tau}\right] (-\varepsilon_G \le \varepsilon < -\varepsilon_c) \quad (32)$$

For $-\varepsilon_G \le \varepsilon < -\varepsilon_c$, mean-field and critical percolation govern on length scales smaller and larger than ξ_G, respectively. Then, the complex modulus has contributions from (1) Rouse relaxation of the precursor chain, (2) Rouse relaxation of the subcluster formed from mean-field percolation, and (3) Rouse relaxation from the MF subcluster to the whole cluster formed from critical percolation (subscript "CP").

$$G^*(\omega) = G_X^*(\omega) + G_{MF}^*(\omega) + G_{CP}^*(\omega)$$
$$= i\omega vkT\left[\sum_{p=2}^{N_X} \frac{\tau_X/p^2}{1 + i\omega\tau_X/p^2} + \frac{N_X - 1}{N_X}\int_{\tau_X}^{\infty} \frac{(\tau_X/\tau)^1}{i\omega + 1/\tau_G + 1/\tau}\frac{d\tau}{\tau} + \frac{0.67}{N_X}\int_{\tau_G}^{\infty} \frac{(\tau_G/\tau)^{0.67}}{i\omega + 1/(\lambda\tau_c) + 1/\tau}\frac{d\tau}{\tau}\right] (-\varepsilon_c \le \varepsilon < \varepsilon_c) \quad (33)$$

For $-\varepsilon_c \le \varepsilon < \varepsilon_c$, the only difference from eq 32 is the cutoff frequency is $\lambda\tau_c$ for the CP part, with $\tau_c = \tau_X^{0.25}\tau_s^{0.75}$ (eq 27) the characteristic time of the critical cluster. Here, λ is a fitting parameter of order unity. Introduction of this prefactor is reasonable considering that τ_c is obtained based on scaling.

$$G^*(\omega) = G_X^*(\omega) + G_{MF}^*(\omega) + G_{CP}^*(\omega) + G_N^*$$
$$= i\omega vkT\left[\sum_{p=2}^{N_X} \frac{\tau_X/p^2}{1 + i\omega\tau_X/p^2} + \frac{N_X - 1}{N_X}\int_{\tau_X}^{\infty} \frac{(\tau_X/\tau)^1}{i\omega + 1/\tau_G + 1/\tau}\frac{d\tau}{\tau} + \frac{0.67}{N_X}\int_{\tau_G}^{\infty} \frac{(\tau_G/\tau)^{0.67}}{i\omega + 1/\tau_{strand} + 1/\tau}\frac{d\tau}{\tau} + \frac{(\varepsilon/\varepsilon_G)^{2.7}}{N_X}\frac{\tau_{life}}{1 + i\omega\tau_{life}}\right]$$
$$(\varepsilon_c \le \varepsilon < \varepsilon_G) \quad (34)$$

For $\varepsilon_c \le \varepsilon < \varepsilon_G$, the complex modulus has contributions from (1) the Rouse relaxation of precursor chains, (2) the Rouse relaxation of substrands formed by mean-field percolation (3) the Rouse relaxation from MF substrands to the whole strand formed by critical percolation, with $1/\tau_{strand}$ the characteristic frequency of a strand, and (4) a gel plateau with amplitude given by eq 24 that relaxes at relaxation time τ_{life} given by eq 30.

$$G^*(\omega) = G_X^*(\omega) + G_{MF}^*(\omega) + G_N^*$$
$$= i\omega vkT\left[\sum_{p=2}^{N_X} \frac{\tau_X/p^2}{1 + i\omega\tau_X/p^2} + \int_{\tau_X}^{\infty} \frac{(\tau_X/\tau)^1}{i\omega + 1/\tau_{strand} + 1/\tau}\frac{d\tau}{\tau} + \varepsilon^3\frac{\tau_{life}}{1 + i\omega\tau_{life}}\right]$$
$$(\varepsilon_G \le \varepsilon < 1) \quad (35)$$

For $\varepsilon_G \le \varepsilon < 1$, the modulus has contributions from (1) the Rouse relaxation of precursor chains, (2) the Rouse relaxation of strands formed by mean field percolation, and (3) a gel plateau with amplitude given by eq 20 that relaxes at relaxation time τ_{life} given by eq 26.

$$G^*(\omega) = G_X^*(\omega) + G_{SR}^*(\omega)$$
$$= i\omega vkT\left[\sum_{p=\varepsilon+1}^{N_X} \frac{\tau_X/p^2}{1 + i\omega\tau_X/p^2} + \sum_{p=1}^{\varepsilon} \frac{\tau_s\varepsilon^2/p^2}{1 + i\omega\tau_s\varepsilon^2/p^2}\right]$$
$$(1 \le \varepsilon) \quad (36)$$

For $1 \le \varepsilon$, the modulus is given by the sticky Rouse model.[14,16] Since the number of sticky Rouse segments per chain $\sim \varepsilon$, the complex modulus is written as a combination of high-order Rouse modes with $N_X \ge p > \varepsilon$ with Rouse time τ_X and low-order sticky Rouse modes (subscript "SR") with $\varepsilon \ge p \ge 1$ that are delayed by ion associations with lifetime τ_s.

3. EXPERIMENTAL SECTION

3.1. Materials. Two narrow molecular weight polystyrenes (PS), M_w = 4000 and 13 500 Da, were obtained from Pressure Chemical Co. and sulfonated in dichloroethane (DCE) using acetyl sulfate.[17] The homogeneous solution sulfonation produces random substitution of sulfonic acid group at the para-position of the phenyl ring.[18] The acetyl sulfate was prepared by slowly adding concentrated sulfuric acid to a 60% excess of acetic anhydride in 1,2-dichloroethane at 0 °C. The freshly prepared acetyl sulfate was added to a stirred 10% solution of PS in DCE at ∼50 °C. The reaction was terminated after 1 h by the addition of 2-propanol. The sulfonated polystyrene (SPS) was isolated by steam distillation of the solvent, washed three times with boiling water, dried in air at 70 °C for 1 day, and finally dried at 120 °C in a vacuum oven for 1 week. The sulfonation level was determined by elemental sulfur analysis at Galbraith Laboratories, Inc.

Three sulfonation levels were prepared for SPS4000, 2.5, 4.8, and 6.5 mol %, and there were two sulfonation levels for the SPS13500, 0.76, and 2.7 mol %. The average number of ionic groups per chain was designed to be 1, 2, and 2.5 for the three SPS4000 ionomers and 1 and 3.5 for the SPS13500, though since sulfonation proceeds randomly, the products are random distributions of chains with varying sulfonation. Alkali metal salts of SPS were prepared by adding a 50% excess of the appropriate metal hydroxide or acetate to the SPS acid derivative in a 90/10 (v/v) mixture of toluene and methanol. The neutralized ionomer was recovered by steam distillation, washed, and dried.

Linear viscoelasticity (LVE) measurements were conducted on either a TA Instruments advanced rheometric expansion system (ARES) or an ARES-G2 rheometer. The samples were prepared by compression molding at 210−250 °C under vacuum, and all experiments were run under nitrogen protection. Parallel plate fixtures of 25 and 8 mm were used for LVE measurements in a T range of 105−260 °C and a frequency range of 0.06−400 rad/s. All

DOI: 10.1021/ma502280g
Macromolecules 2015, 48, 1221−1230

measurements were made within the linear regime as confirmed from strain sweep experiments.

Previous studies constructed master curves for the polystyrene (PS4000) and sulfonated polystyrene (SPS4000) ionomers at reference temperatures of $T_r \approx T_g + 45$ °C, where $T_r \approx 140$ °C for the high ionic content samples of 4.8 and 6.5 mol %. For comparison, the master curves were constructed for the PS13500, and SPS13500 ionomers at reference $T_r = 140$ °C.

4. RESULTS AND DISCUSSION

4.1. Overview. Figures 4a, 4b, and 4c show the master curves of storage and loss modulus at $T_r \approx T_g + 45$ °C for PS4000 and SPS4000 with ionic contents of 2.5 mol % ($\varepsilon = -0.064$), 4.8 mol % ($\varepsilon = 0.80$), and 6.5 mol % ($\varepsilon = 1.4$), respectively. Figures 5a and 5b show the master curves storage and loss modulus at $T_r = 140$ °C for PS13500 and SPS13500 with ionic contents of 0.76 mol % ($\varepsilon = -0.026$) and 2.7 mol % ($\varepsilon = 2.5$), respectively.

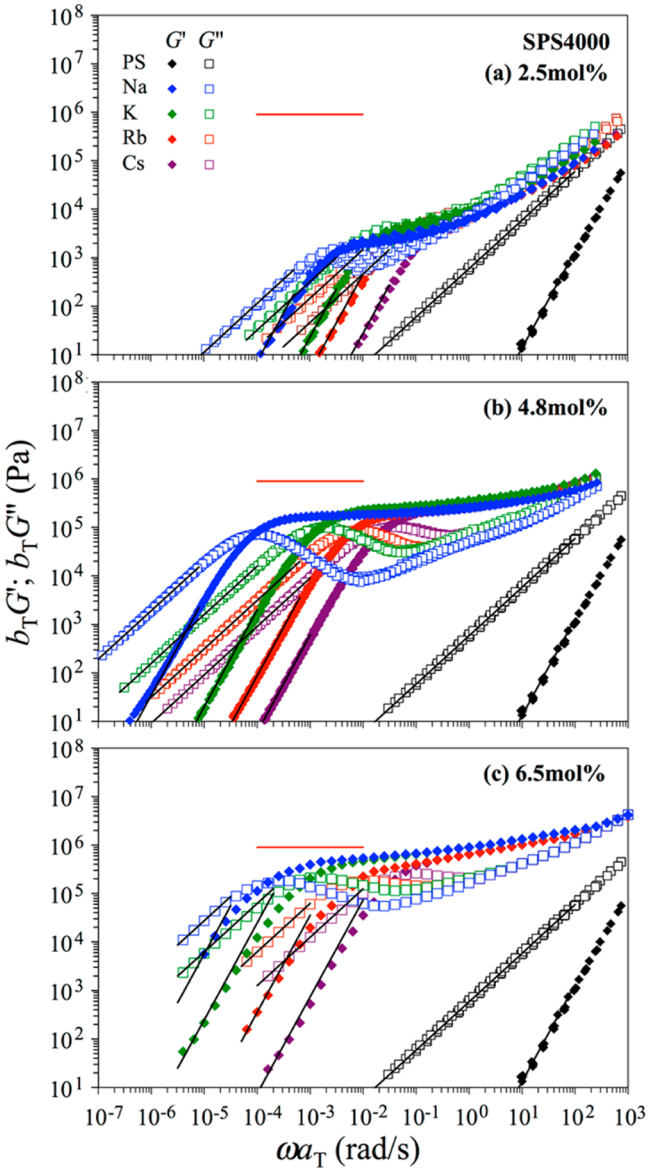

Figure 4. Frequency dependence of storage and loss moduli, G' and G'', master curves at $T_r \approx T_g + 45$ °C for randomly sulfonated PS4000 with contents of sulfonated monomers: (a) 2.5, (b) 4.8, and (c) 6.5 mol %. The solid lines associated with G' and G'' are terminal tails $G' \propto \omega^2$ and $G'' \propto \omega$ used to calculate the viscosity, recoverable compliance, and relaxation times in Table 1. The red lines indicate vkT.

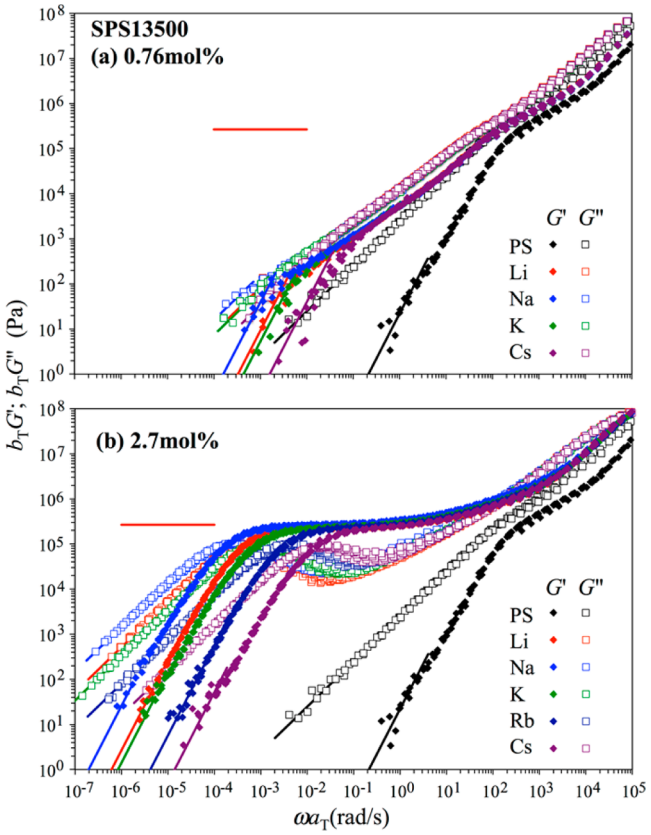

Figure 5. Frequency dependence of storage and loss moduli, G' and G'', master curves at $T_r = 140$ °C for randomly sulfonated PS13500 with contents of sulfonated monomers: (a) 0.76 and (b) 2.7 mol %. The solid lines associated with G' and G'' are terminal tails $G' \propto \omega^2$ and $G'' \propto \omega$ used to calculate the viscosity, recoverable compliance, and relaxation times in Table 2. The red lines indicate vkT.

For each ionic content, G' and G'' are compared for ionomers having various alkali counterions: lithium (Li), sodium (Na), potassium (K), rubidium (Rb), and cesium (Cs). It is obvious the relaxation behavior is quite different for SPS4000 2.5 mol % samples compared with SPS4000 4.8 mol % and 6.5 mol % samples (Figure 4) and SPS13500 0.76 mol % samples compared with SPS13500 2.7 mol % samples (Figure 5): The SPS4000 2.5 mol % and SPS13500 0.76 mol % samples show power law like relaxation with very low terminal moduli (much lower than vkT indicated by the red line), suggesting the gel has not yet been well formed, while the SPS4000 4.8 mol %, 6.5 mol %, and SPS13500 2.7 mol % samples show a clear plateau corresponding to the gel structure. This result supports the gel point estimated via eq 1, $p_c = 2.7$ mol % for SPS4000 and $p_c = 0.78$ mol % for SPS13500 are reasonable.

In particular, for the SPS13500 0.76 mol % samples, the storage modulus is plotted against ω in Figure 6, where three power law regions can be observed from high to low frequency: (1) the precursor chain Rouse region where $G'(\omega) \sim \omega^{1/2}$, (2) the mean-field gelation region where $G'(\omega) \sim \omega^1$, and (3) the critical percolation region where $G'(\omega) \sim \omega^{0.67}$, followed by the terminal relaxation $G'(\omega) \sim \omega^2$. This result rationalizes the incorporation of the Ginzburg point in section 2.

DOI: 10.1021/ma502280g
Macromolecules 2015, 48, 1221−1230

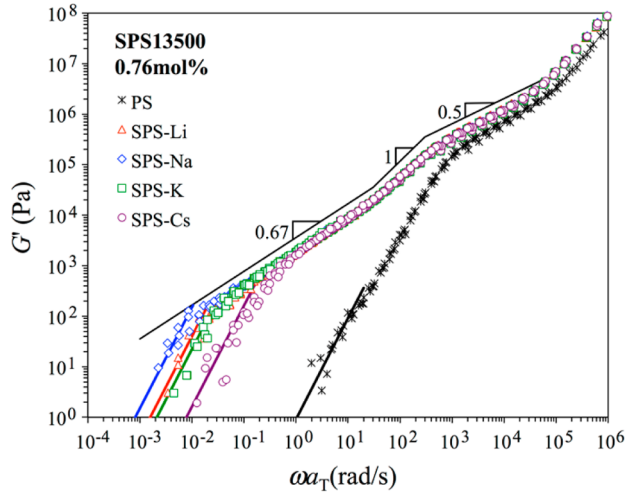

Figure 6. Frequency dependence of storage modulus G' master curves at T_r = 140 °C for randomly sulfonated PS13500 with contents of 0.76 mol %. The thin solid lines above the curve show the power law regions (1) $G' \propto \omega^{0.5}$, (2) $G' \propto \omega^{1}$, and (3) $G' \propto \omega^{0.67}$ before terminal relaxation $G' \propto \omega^{2}$ shown as thick solid lines.

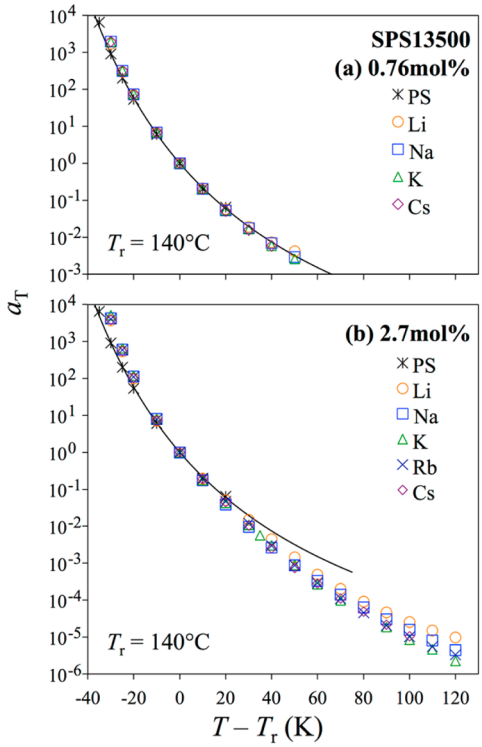

Figure 7. Shift factor a_T against $T - T_r$ for randomly sulfonated SPS13500 with contents of sulfonated monomers: (a) 0.76 and (b) 2.7 mol %. The solid curves are the WLF equation of PS: log a_T = $-8.07(T - T_r)/(111.6 + T - T_r)$ with T_r = 140 °C.

4.1. Time−Temperature Superposition. Before detailed discussion of the master curves, a comment is needed on the time−temperature superposition (tTs) utilized to construct the master curves. It should be noted that the tTs failed in a transition region from the Rouse modulus to the network modulus; see the valley region of G'' in Figures 4 and 5. This failure is expected because for the Rouse part and the network part, the modulus is governed by τ_X and τ_s, respectively, where τ_X and τ_s necessarily have different T dependences, since $\tau_s = \tau_0 \exp(E_a/kT)$, where τ_0 is the relaxation time of a Kuhn segment and E_a the activation energy.[14]

Figure 7 shows the shift factors, corresponding to the SPS13500 data in Figure 5, plotted against $T - T_r$ (T_r = 140 °C). The temperature dependence of the 2.7 mol % samples at $T - T_r \geq 40$ °C ($T \geq 180$ °C) deviate strongly from the Williams−Landel−Ferry (WLF) equation for PS: log a_T = $-8.07(T - T_r)/(111.6 + T - T_r)$ with T_r = 140 °C, where the modulus is governed by the network part controlled by τ_s. This type of deviation of T dependence from neutral samples was reported previously as being due to a stronger T dependence of τ_s compared with that of τ_0.[14] For the SPS4000 samples, only those relaxation modes slower than the relaxation of the precursor chain are measured, so a change of temperature dependence (from that of τ_0 to that of τ_s) is not clearly seen.

4.2. Relaxation Time. The solid lines fit to the low frequency G' and G'' data in Figures 4 and 5 denote the terminal tails of $G' \propto \omega^2$ and $G'' \propto \omega$. From these tails, the zero-shear viscosity can be obtained as

$$\eta_0 = \lim_{\omega \to 0}\left[\frac{G''(\omega)}{\omega}\right] \tag{37}$$

The steady-state recoverable compliance as

$$J_e = \lim_{\omega \to 0}\left\{\frac{G'(\omega)}{[G''(\omega)]^2}\right\} \tag{38}$$

and the weight-average relaxation time as[19]

$$\tau = \eta_0 J_e = \lim_{\omega \to 0}\left[\frac{G'(\omega)}{\omega G''(\omega)}\right] \tag{39}$$

The values of η_0, J_e, and τ obtained for SPS ionomers in Figures 4 and 5 are listed in Tables 1 and 2, respectively.

In both Figures 4 and 5, it is noted that the relaxation time increases with decreasing the counterion size, except the Li counterion data deviate from this trend. The trend is in accordance with a simple expectation that the lifetime of ionic association increases with ion interaction energy, which increases as counterion size decreases.[7,8]

Since p = 2.5 mol % of the SPS4000 samples and p = 0.76 mol % of SPS13500 samples are very close to their gel points p_c = 2.7 and 0.78 mol %, respectively, their terminal relaxations likely occur by effective breakup. These two samples correspond to $-\varepsilon_c \leq \varepsilon < 0$, where clusters relax by Rouse motion until effective breakup at τ_c. This expectation can be tested quantitatively via $\tau_c \propto \tau_X^{1/4}\tau_s^{3/4}$ (eq 27). On one hand, τ_X = 2.2 × 10^{-4} and 9.0 × 10^{-3} s for PS4000 and PS13500, respectively. On the other hand, τ_s can be estimated as the relaxation time divided by ε^2 where $\varepsilon > 1$ (see eq 16), i.e., SPS4000 of 6.5 mol % (ε = 1.4) and SPS13500 of 2.7 mol % (ε = 2.5) samples. In Figure 8, τ_c (τ of SPS4000 of 2.5 mol % and SPS13500 of 0.76 mol %) is plotted against $\tau_X^{0.25}\tau_s^{0.75}$, with each point corresponding to one counterion. The proportionality is well observed, which supports the relaxation by effective breakup assigned for the SPS4000 of 2.5 mol % and SPS13500 of 0.76 mol % samples close to their gel points.

4.3. Comparison with the Model Predictions. To quantitatively test the relaxation mechanism, Figure 9 compares the model prediction and experimental results of all sets of samples having the same K^+ counterion. (Comparison for

DOI: 10.1021/ma502280g
Macromolecules 2015, 48, 1221−1230

Table 1. η_0, J_e, and τ of SPS Ionomers Having M = 4000 with Different Ionic Contents and Counterions at $T_r \approx T_g$ + 45 °C

	2.5 mol %			4.8 mol %			6.5 mol %		
	η_0(Pa s)	J_e (Pa^{-1})	τ (s)	η_0(Pa s)	J_e (Pa^{-1})	τ (s)	η_0(Pa s)	J_e (Pa^{-1})	τ (s)
Na	1.1×10^6	5.6×10^{-4}	6.3×10^2	1.9×10^9	9.3×10^{-6}	1.8×10^4	2.8×10^9	7.4×10^{-6}	2.0×10^4
K	3.2×10^5	2.2×10^{-4}	7.1×10^1	1.6×10^8	7.9×10^{-6}	1.3×10^3	6.3×10^8	6.3×10^{-6}	4.0×10^3
Rb	1.4×10^5	2.1×10^{-4}	3.1×10^1	3.2×10^7	8.9×10^{-6}	2.8×10^2	6.3×10^7	8.9×10^{-6}	5.6×10^2
Cs	4.6×10^4	1.3×10^{-4}	5.9	9.1×10^6	7.2×10^{-6}	6.6×10^1	1.3×10^7	4.7×10^{-6}	5.9×10^1

Table 2. η_0, J_e, and τ_w of SPS Ionomers Having M = 13 500 with Different Ionic Contents and Counterions at T_r = 140 °C

	0.76 mol %			2.7 mol %		
	η_0(Pa s)	J_e (Pa^{-1})	τ (s)	η_0(Pa s)	J_e (Pa^{-1})	τ (s)
Li	8.4×10^4	1.3×10^{-3}	1.1×10^2	5.1×10^8	1.0×10^{-5}	5.1×10^3
Na	1.6×10^5	1.5×10^{-3}	2.3×10^2	1.5×10^9	1.2×10^{-5}	1.7×10^4
K	7.3×10^4	9.8×10^{-4}	7.2×10^1	3.4×10^8	1.3×10^{-5}	4.2×10^3
Rb				8.0×10^7	8.9×10^{-6}	7.1×10^2
Cs	3.3×10^4	3.6×10^{-4}	1.2×10^1	1.6×10^7	2.0×10^{-5}	3.2×10^2

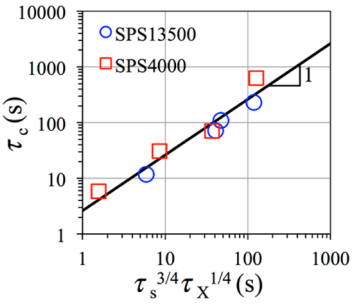

Figure 8. Test of effective breakup time for SPS4000 and SPS13500 ionomers (eq 27). τ_X is the relaxation time of the precursor chain. τ_s is estimated as the relaxation time divided by ε^2 for samples far above the gel point, i.e., SPS4000 ionomer with p = 6.5 mol % and SPS13500 ionomer with p = 2.7 mol %. τ_c is estimated as the relaxation time for samples near the gel point, i.e., SPS4000 ionomer with p = 2.5 mol % and SPS13500 ionomer with p = 0.76 mol %. Solid line is a linear fit yielding $\tau_c = 2.6\tau_s^{3/4}\tau_X^{1/4}$.

ionomers with Na^+, Rb^+, and Cs^+ as counterions are shown in the Supporting Information.) For the PS samples, the prediction is given by the Rouse model with only one fitting parameter τ_0, the Rouse time for a Kuhn segment. For the ionomers, the model prediction is based on eq 33 with λ = 5 (for SPS4000 of 2.5 mol % and SPS13500 of 0.76 mol %), eq 35 (for SPS4000 of 4.8 mol % with ε (= 0.8) > ε_G (= $N_X^{-1/3}$)), and eq 36 (for SPS4000 of 6.5 mol % and SPS13500 of 2.7 mol %) with the two inputs, τ_0 and E_a, give $\tau_s = \tau_0 \exp(E_a/kT)$. τ_0, τ_s, and E_a for different counterions are summarized in Table 3. For Cs counterions, E_a/kT = 14.2, making the dissociated fraction $\exp(-E_a/kT) \sim O(10^{-6})$, justifying the assumption that all the ionic groups are associated, as the smaller counterions have even larger E_a/kT. The number of segments N_X is chosen as the number of Kuhn segments based on molecular weight M_K = 850 g/mol for each segment.[20] ε values utilized in the model calculation were directly obtained from eqs 1 and 2.

For SPS4000 of 2.5 mol %, the modulus is not strictly a power of 0.67 before the terminal relaxation. Comparison of G' of the SPS4000 of 2.5 mol % and SPS13500 of 0.76 mol % samples reveals a small plateau for the former before the terminal relaxation. The molecular origin of the plateau is still not clear. Since the relaxation near the gel point becomes very sensitive to a small change of the degree of sulfonation, a small underestimation of p may lead to a big change in LVE response.

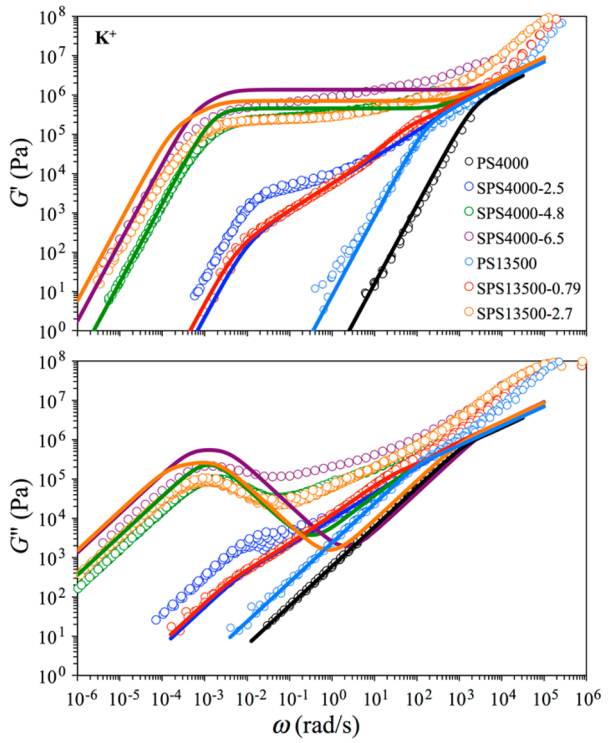

Figure 9. Storage and loss moduli, G' and G'', plotted against ω for K neutralized SPS4000 of 2.5 and 4.8 mol % at $T = T_g$ + 45 °C and SPS4000 of 6.5 mol % and SPS13500 of 0.76 and 2.7 mol % at T = 140 °C. The solid curves are the model predictions.

Table 3. τ_0, τ_s, and E_a Utilized in Model Calculation for SPS Samples Shown in Figure 9 and Figures S1−S3[a]

	PS4000	PS13500	Na	K	Rb	Cs
τ_0 (μs)	18	20	32	32	32	32
τ_s (s)			4500	770	160	47
E_a/kT			18.8	17.0	15.4	14.2

[a]The reference temperature T_rs are listed in Table 2 of ref 7 for PS4000 and SPS4000 of 2.5 and 4.8 mol %; T_r = 140 °C for SPS4000 of 6.5 mol %, PS13500, and SPS13500 of 0.76 and 2.7 mol %.

In fact, the relaxation modulus can be better predicted by slightly adjusting p to 3.0 mol % for SPS4000.

DOI: 10.1021/ma502280g
Macromolecules 2015, 48, 1221−1230

Although a small deviation is noted for SPS4000 of 2.5 mol %, the model prediction shown in Figure 9 captures well the change of LVE for the K^+ neutralized samples with gelation, with the same τ_0 and τ_s (see Table 3). This agreement strongly supports the view presented above for the structure of the ionomer near the gel point: the precursor chains are connected in a mean-field way on local scales smaller than the Ginzburg blob, but connected in a critical percolation way on length scales larger than the Ginzburg blob. For those samples above the gel point, there are obviously some relaxation modes between the Rouse and ionic dissociation not predicted in the model presented here. These modes are likely to be contributed from dangling ends in the gel as well as size distributions of the gel strands not incorporated herein. (Since the systems considered here are nonentangled, the dangling ends should not affect LVE as strongly as predicted by the Curro−Pincus model.[21])

5. CONCLUSIONS

Using standard percolation theory for gelation that includes both critical and mean-field regimes, the linear viscoelastic response of lightly sulfonated short polystyrene is quantitatively understood. LVE changes drastically in the vicinity of the gel point, corresponding to an average of one cross-link per chain. Very close to the gel point the effective breakup ideas of Rubinstein and Semenov appear to control the terminal relaxation. The association lifetime and energy both are found to increase logically as counterions get smaller.

This work is the first precise control of sulfonated polystyrene very close to the gel point where $p \sim p_c \sim 1/(N-1)$ corresponding to one ionic group per chain on average. Most previously studied sulfonated polystyrene samples have p much higher than p_c and hence are not suitable to test the sol−gel transition.[15,22−24] These samples show typical reversible gel behavior characterized by clear plateaus and delayed relaxation governed by the association lifetime τ_s and will be the subject of a future publication.

APPENDIX

In general, the larger a cluster/strand, the smaller its breakup time while the larger its Rouse time. Therefore, there is a critical cluster/strand for which the breakup time and Rouse time are equal. This time was defined by Rubinstein and Semenov as the effective breakup time.[9,10]

For $\varepsilon_c > \varepsilon_G$, the mean-field percolation holds at ε close to ε_c. Therefore, τ_c can be conveniently determined in Figure 10 from the cross point of the solid blue line for the Rouse relaxation of clusters formed from the mean-field percolation and the blue dashed line for the effective breakup of strands formed from the mean-field percolation:

$$G = \nu kT\omega\tau_X \quad \text{solid blue line} \tag{A1}$$

$$G = \nu kT(\omega\tau_s)^{-3} \quad \text{dashed blue line} \tag{A2}$$

Equations A1 and A2 equate at $\omega_c = \tau_X^{-1/4}\tau_s^{-3/4}$ (i.e., $\tau_c = \tau_X^{1/4}\tau_s^{3/4}$) and $G_c = \nu kT(\tau_X/\tau_s)^{3/4}$. Similarly, in the case of $\varepsilon_c < \varepsilon_G$, the critical percolation holds at ε close to ε_c. Therefore, τ_c can be conveniently determined from the cross point of the solid red line for the Rouse relaxation of critical percolation clusters and the red dashed line for the effective breakup of strands formed by critical percolation, with θ (>0) an exponent to be determined below.

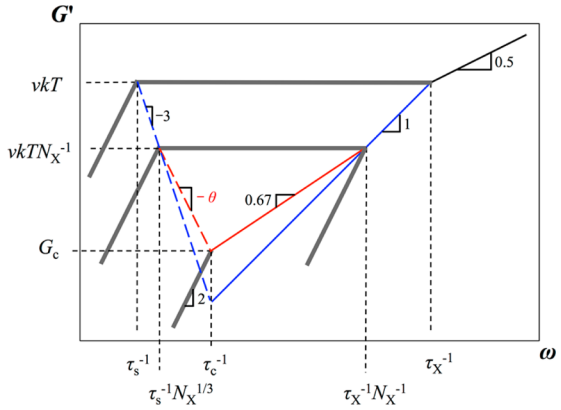

Figure 10. Schematic determination of effective breakup time τ_c in the two cases of $\varepsilon_c > \varepsilon_G$ (blue lines) where the effective breakup works on mean-field clusters/strands and $\varepsilon_c < \varepsilon_G$ (red lines) where the effective breakup works on critical percolation clusters/strands.

$$G = \frac{\nu kT}{N_X}(\omega\tau_X N_X)^{2/3} \quad \text{solid red line} \tag{A3}$$

$$G = \frac{\nu kT}{N_X}(\omega\tau_s N_X^{-1/3})^{-\theta} \quad \text{dashed red line} \tag{A4}$$

Equations A3 and A4 equate at $\omega_c = \tau_X^{-2/(2+3\theta)} \times \tau_s^{-3\theta/(2+3\theta)} \times N_X^{-(2-\theta)/(2+3\theta)}$ and $G_c = \nu kT \times (\tau_X/\tau_s)^{2\theta/(2+3\theta)} \times N_X^{(-6-\theta)/(6+9\theta)}$. Since N_X has been properly accounted in τ_X, it is reasonable to require the N_X exponent to equal 0 in the expression of ω_c to give $\theta = 2$, and accordingly $\tau_c = \omega_c^{-1} = \tau_X^{1/4}\tau_s^{3/4}$ and $G_c = \nu kT(\tau_X/\tau_s)^{1/2}N_X^{-1/3}$. Note that the expression of τ_c is the same as that determined for $\varepsilon_c > \varepsilon_G$.

ASSOCIATED CONTENT

Supporting Information

Figures S1−S4. This material is available free of charge via the Internet at http://pubs.acs.org.

AUTHOR INFORMATION

Corresponding Author

*E-mail: chenquant@gmail.com (Q.C.).

Notes

The authors declare no competing financial interest.

ACKNOWLEDGMENTS

Q.C. and R.H.C. acknowledge the Division of Materials Research Polymers Program at the National Science Foundation (Grant DMR-1404586) for financial support. C.H. and R.A.W. acknowledge the financial support of the Chemical, Bioengineering, Environmental, and Transport Systems (CBET) Division of the Directorate of Engineering at the National Science Foundation (Grant CBET 1066517).

REFERENCES

(1) Nijenhuis, K. T. *Adv. Polym. Sci.* **1997**, *130*, 1−12.
(2) Flory, P. J. *Introductory Lecture*; Faraday Division, Chemical Society: London, 1974; Vol. 57.
(3) Rubinstein, M.; Colby, R. H. *Polymer Physics*; Oxford University Press: New York, 2003.
(4) He, Q.; Harwell, M. G.; Hung, J.; Martin, K. E.; Iqbal, T.; Samuels, S. L. Ionomer-Containing Hot Melt Adhesive. WO2005078037, 2005.

DOI: 10.1021/ma502280g
Macromolecules 2015, 48, 1221−1230

(5) Sakakibara, K.; Fukumoto, M. Method and Device for Diagnosing Rechargeable Batteries. US20050017686, 2004.
(6) Chen, Q.; Colby, R. H. *Korea−Australia Rheol. J.* **2014**, *26* (3), 257−261.
(7) Weiss, R. A.; Zhao, H. Y. *J. Rheol.* **2009**, *53* (1), 191−213.
(8) Ling, G. H.; Wang, Y. Y.; Weiss, R. A. *Macromolecules* **2012**, *45* (1), 481−490.
(9) Rubinstein, M.; Semenov, A. N. *Macromolecules* **1998**, *31* (4), 1386−1397.
(10) Semenov, A. N.; Rubinstein, M. *Macromolecules* **1998**, *31* (4), 1373−1385.
(11) Derosa, M. E.; Winter, H. H. *Rheol. Acta* **1994**, *33* (3), 220−237.
(12) Lusignan, C. P.; Mourey, T. H.; Wilson, J. C.; Colby, R. H. *Phys. Rev. E* **1995**, *52* (6), 6271−6280.
(13) Rubinstein, M.; Colby, R. H. *Macromolecules* **1994**, *27* (12), 3184−3190.
(14) Chen, Q.; Tudryn, G. J.; Colby, R. H. *J. Rheol.* **2013**, *57* (5), 1441−1462.
(15) Colby, R. H.; Zheng, X.; Rafailovich, M. H.; Sokolov, J.; Peiffer, D. G.; Schwarz, S. A.; Strzhemechny, Y.; Nguyen, D. *Phys. Rev. Lett.* **1998**, *81* (18), 3876−3879.
(16) Chen, Q.; Liang, S.; Shiau, H.-S.; Colby, R. H. *ACS Macro Lett.* **2013**, *2* (11), 970−974.
(17) Makowski, H. S.; Lundberg, R. D.; Singhal, G. H. Flexible polymeric compositions comprising a normally plastic polymer sulfonated to about 0.2 to about 10 mol % sulfonate. US3870841, 1975.
(18) Zhang, L. H.; Katzenmeyer, B. C.; Cavicchi, K. A.; Weiss, R. A.; Wesdemiotis, C. *ACS Macro Lett.* **2013**, *2* (3), 217−221.
(19) Graessley, W. W. *Adv. Polym. Sci.* **1974**, *16*, 1−179.
(20) Inoue, T.; Osaki, K. *Macromolecules* **1996**, *29* (5), 1595−1599.
(21) Curro, J. G.; Pincus, P. *Macromolecules* **1983**, *16* (4), 559−562.
(22) Eisenberg, A.; Kim, J.-S. *Introduction to Ionomers*; Wiley: New York, 1998.
(23) Eisenberg, A.; Hird, B.; Moore, R. B. *Macromolecules* **1990**, *23* (18), 4098−4107.
(24) Weiss, R. A.; Yu, W. C. *Macromolecules* **2007**, *40* (10), 3640−3643.

DOI: 10.1021/ma502280g
Macromolecules 2015, 48, 1221−1230